Modeling of Quasi-Optical Systems and Measurements with a Cobot in the J-Band

Gregory Gaudin, Daniel Bourreau, Clément Henry, Alain Peden

▶ **To cite this version:**

Gregory Gaudin, Daniel Bourreau, Clément Henry, Alain Peden. Modeling of Quasi-Optical Systems and Measurements with a Cobot in the J-Band. 18th European Conference on Antennas and Propagation (EuCAP2024), Mar 2024, Glasgow, United Kingdom. 10.23919/EuCAP60739.2024.10501609 . hal-04615494

HAL Id: hal-04615494
https://hal.science/hal-04615494v1

Submitted on 18 Jun 2024

HAL is a multi-disciplinary open access archive for the deposit and dissemination of scientific research documents, whether they are published or not. The documents may come from teaching and research institutions in France or abroad, or from public or private research centers.

L'archive ouverte pluridisciplinaire **HAL**, est destinée au dépôt et à la diffusion de documents scientifiques de niveau recherche, publiés ou non, émanant des établissements d'enseignement et de recherche français ou étrangers, des laboratoires publics ou privés.

Distributed under a Creative Commons Attribution - NonCommercial - NoDerivatives 4.0 International License

Modeling of Quasi-Optical Systems and Measurements with a Cobot in the J-Band

Gregory Gaudin*†, Daniel Bourreau*†, Clément Henry*† Alain Peden*†,
*Dept Microwave, IMT Atlantique, Brest, France
†Lab-STICC, UMR CNRS 6285, Brest, France

***Abstract*—Terahertz waves bring together the assets of microwave and infrared waves and open up new possibilities in structure analysis and material characterization. In order to optimize a J-band material characterization bench (220-330 GHz), this work proposes a novel simulation tool based on a Gaussian beam formalism enabling the modeling and design of large size quasi-optical components. Numerical results showing the applicability of this framework in the modeling of a J-band lens antenna are provided and validated through measurements performed with a robotic bench.**

***Index Terms*—diagonal horn, propagation, THz, Gaussian beam, field expansion, beam tracing, GOLA, cobot, measurements.**

I. Introduction

Quasi-optical techniques for free-space material characterization are really attractive as broadband permittivity extraction can be performed especially at very high frequencies such as in the W-, D- or J-band. Moreover, these techniques enable the characterization of solid materials without any specific machining of the sample under test as it would be required with rectangular or coaxial waveguide cells or cavities. Non-solid material characterization is also available using a specific container. Therefore, a quasi-optical experimental setup along with a calibration procedure and data processing software allows the precise extraction of the material relative permittivity [1]. Current characterizations are performed assuming that the material under test (MUT) is large enough to intercept the incident beam under a normal incidence and that the beam is paraxial, yielding a planar wavefront at the MUT surface. To evaluate the potential impact of such approximations, an option is to model electromagnetically the quasi-optical (QO) components of the bench (e.g. horns, lenses, mirrors). Commercial software packages like HFSS, CST, or FEKO are inadequate for this specific setting due to the large electrical component size at these frequencies, resulting in prohibitively long simulation times in the design of the test bench.

The following study focuses on the modelling of highly directive Gaussian Optic Lens Antennas (GOLA), which are key components of the J-band free-space characterization bench. Gaussian beam formalism [2], commonly employed in laser optics, can be used to decompose an arbitrary electromagnetic field into elementary beams [3], allowing for beam launching to describe the propagation and interaction of the electromagnetic field through the QO system [4].

Methods and models for simulating QO systems will be initially presented. The simulation results will then be discussed and compared with preliminary measurements performed in the J-band.

II. Simulation of quasi-optical systems

A. Principle

This section assumes that the aperture fields at the horn feeding the system have already been computed with the use of a mode-matching technique, presented in [5] and [6]

Fig. 1 illustrates the three main stages of the simulation: field expansion (GBE), beam tracing (GBT), and beam summation (GBS). The core element of the tool is the Vectorial Astigmatic Gaussian Beam [4], which is defined as

$$u(x,y,z) = u_0(z)\cdot\exp\left\{-j\frac{k}{2}\begin{bmatrix}x & y\end{bmatrix}\mathbf{Q}(z)\begin{bmatrix}x\\y\end{bmatrix}+j\phi(z)\right\}. \tag{1}$$

The complex curvature matrix $\mathbf{Q}$ and the complex phase are detailed in [4]. The equation given in [7, eq. 1.9] can be rewritten, using a factorization by $u(x,y,z)$, as

$$\vec{E}_{gb}(x,y,z) = \begin{bmatrix}\alpha_x\\ \alpha_y\\ -\frac{1}{2}\begin{bmatrix}\alpha_x & \alpha_y\end{bmatrix}\left(\mathbf{Q}(z)+\mathbf{Q}^t(z)\right)\begin{bmatrix}x\\y\end{bmatrix}\end{bmatrix} u(\boldsymbol{r}), \tag{2}$$

in which $\boldsymbol{r}\in\mathbb{R}^3$ is the position vector. Equations 1 and 2 should be applied within the local reference frame of the beam, where $\hat{\boldsymbol{z}}$ denotes the direction of beam propagation.

B. Field expansion and beam summation

The electromagnetic field $\boldsymbol{E}_s$ received at sampled points $\boldsymbol{r}_p$ on a surface can be expressed as a sum of N vectorial Gaussian beams, as described in [3]. Each of these beams is further separated into XZ and YZ polarizations,

$$\boldsymbol{E}_{gb,n} = \alpha_{x,n}\boldsymbol{E}_{xz,n} + \alpha_{y,n}\boldsymbol{E}_{yz,n}, \tag{3}$$

and is oriented towards the Poynting vector of the incoming field at the sampled point n ($n\in[1,N]$), which is along the local $\hat{\boldsymbol{z}}$ axis.

In matrix form, Equation 4 represents the linear system that needs to be solved, as outlined in [3]. Solving

$$\begin{bmatrix}\mathbf{E}_{xz\cdot x} & \mathbf{E}_{xz\cdot y}\\ \mathbf{E}_{yz\cdot x} & \mathbf{E}_{yz\cdot y}\end{bmatrix}\begin{bmatrix}\vec{\alpha}_x\\ \vec{\alpha}_y\end{bmatrix} = \begin{bmatrix}\vec{E}_{s\cdot x}\\ \vec{E}_{s\cdot y}\end{bmatrix}, \tag{4}$$

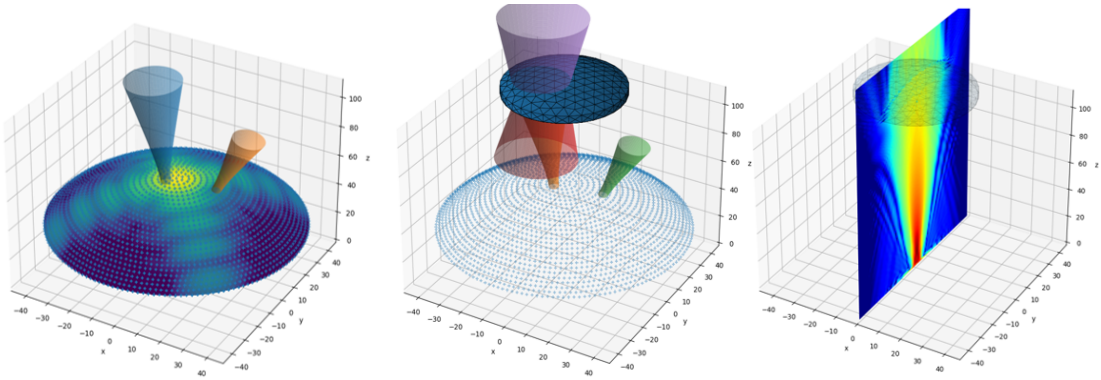

(a) Field expansion (b) Beam tracing (c) Beam summation

Fig. 1. Main steps of a simulation using gaussian beams.

yields the following polarization coefficients for each beam, with (same applies for YZ polarization):

$$\mathbf{E}_{xz\cdot x} = \begin{bmatrix} \boldsymbol{E}_{xz,1}(\boldsymbol{r}_1)\cdot\hat{\boldsymbol{x}}_1 & \dots & \boldsymbol{E}_{xz,N}(\boldsymbol{r}_1)\cdot\hat{\boldsymbol{x}}_1 \\ \vdots & & \\ \boldsymbol{E}_{xz,1}(\boldsymbol{r}_N)\cdot\hat{\boldsymbol{x}}_N & \dots & \boldsymbol{E}_{xz,N}(\boldsymbol{r}_N)\cdot\hat{\boldsymbol{x}}_N \end{bmatrix} \tag{5a}$$

$$\vec{\alpha}_x = \begin{bmatrix} \alpha_{x,1} \\ \vdots \\ \alpha_{x,N} \end{bmatrix} \tag{5b}$$

$$\vec{E}_{s\cdot x} = \begin{bmatrix} \boldsymbol{E}_s(\boldsymbol{r}_1)\cdot\hat{\boldsymbol{x}}_1 \\ \vdots \\ \boldsymbol{E}_s(\boldsymbol{r}_N)\cdot\hat{\boldsymbol{x}}_N \end{bmatrix}. \tag{5c}$$

The electric field can be determined at any given spatial point by applying the recombination formula,

$$^{g}\boldsymbol{E}(^{g}\boldsymbol{r}) \approx \sum_{n=1}^{N} {}^{g}\mathbf{K}_n \times {}^{n}\boldsymbol{E}_{gb}(^{n}\boldsymbol{r}), \tag{6}$$

in which $^{g}\mathbf{K}_n$ represents the transition matrix between the local frame (n) of the nth beam and the reference frame (g) of the system. Thus, $^{g}\boldsymbol{E}(^{g}\boldsymbol{r})$ denotes the electric field written in the reference frame.

Table I illustrates the influence of the number of beams on both field expansion and beam summation. These tests were carried out on a 12-core processor with parallelism optimizations enabled. As shown, it's not necessary to use an excessively high number of beams to achieve satisfactory results. The median error consistently remains near -40 dB, with a low standard deviation. The reference fields were computed using the Stratton-Shu formula [8, p. 170], and the error was assessed using

$$\text{error} = \frac{|\boldsymbol{E}_{sim} - \boldsymbol{E}_{ref}|}{\max(|\boldsymbol{E}_{ref}|)}. \tag{7}$$

TABLE I
RECOMBINATION ERROR ON THE E-PLANE W.R.T. THE NUMBER OF BEAMS

N	duration GBE [s]	duration GBS* [s]	median error	stdev error
2916	10	45	$1.40 \cdot 10^{-4}$	$8.89 \cdot 10^{-4}$
2116	5	35	$1.33 \cdot 10^{-4}$	$8.62 \cdot 10^{-4}$
1600	3	25	$1.30 \cdot 10^{-4}$	$8.37 \cdot 10^{-4}$
1296	2	20	$1.35 \cdot 10^{-4}$	$7.99 \cdot 10^{-4}$
1024	1.5	17	$1.51 \cdot 10^{-4}$	$7.95 \cdot 10^{-4}$
900	1	14	$2.10 \cdot 10^{-4}$	$8.12 \cdot 10^{-4}$

* xOz plane with 54000 points

C. Beam tracing

Each beam produced through the field expansion undergoes tracking within the quasi-optical system. This step serves a dual purpose: firstly, it aims to identify all points of intersection between the beams and the surfaces of the objects. Secondly, it seeks to determine the complex curvature matrices and polarization coefficients of both reflected and transmitted beams at each interface, as described in [4, p. 6038]. Following this, the reflected and transmitted beams are matched with the incident beam by introducing an additional term into $u(x, y, z)$ (2), where t_0 represents the distance between the origin of the incident beam and the point of intersection. Further details can be found in [9, p. 5].

$$u_g(x, y, z) = u(x, y, z) \cdot \frac{u_{inc}(0, 0, t_0)}{u(\vec{0})} \exp\left\{ j \frac{\phi_{inc}(t_0)}{\phi(0)} \right\} \tag{8}$$

The system can be subdivided into multiple domains (as shown in Fig. 2). At each interface, both forward and backward, beam summation and field expansion (GBE) are conducted.

D. Use case of this paper

The new simulation tool was employed to verify an assumption made in the quasi-optical characterization setup. This bench operates on the premise that the MUT is exposed to a plane wave under normal incidence, using two GOLAs. The

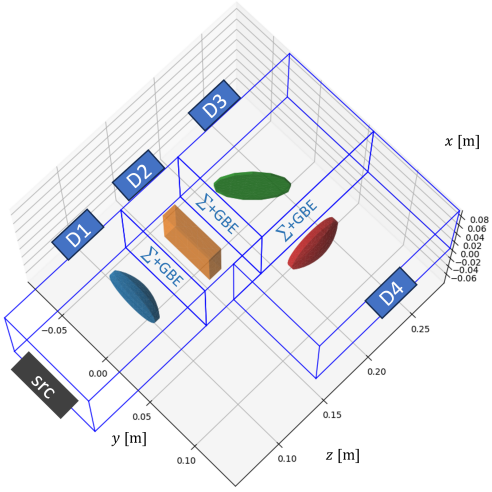

(a) 3D view of the system

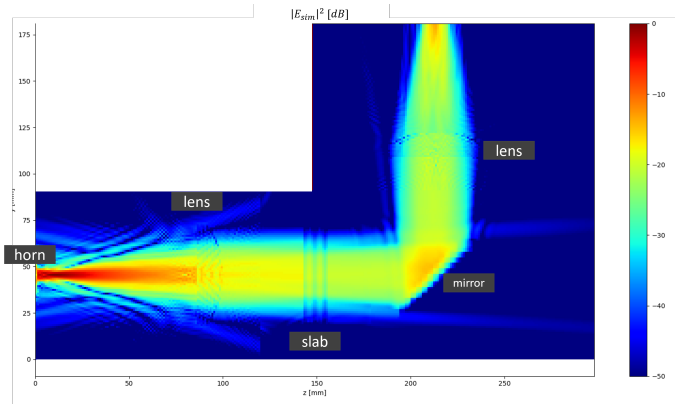

(b) Normalized intensity

Fig. 2. Example of quasi-optical system subdivided in several domains.

primary lobes of these horns generate quasi-Gaussian beams. Consequently, the sole location where this assumption holds true is at the beam waist, where the phase fronts are planar.

Fig. 3 illustrates a simulation in which the lens' entry plane is positioned 85 mm away from the antenna aperture. With this setup, the system generates a collimated beam with nearly flat phase fronts. This configuration is presumed to be optimal for achieving the best results, as the exact positioning of the MUT is not critical. The actual bench indeed employs this distance between the aperture and the lens' entry plane and yields satisfactory results [1].

These simulation results were validated against measurements obtained using a robotic test bench, as presented in the following section.

III. Measurements with a Robotic Test Bench

A. Setup

The bench is divided in two parts. The first part remains stationary and comprises a millimeter-wave converter, a diagonal horn (referred to as the source), and a PTFE lens. The second part consists of a UR10e robotic arm with six degrees of freedom, manufactured by Universal Robot. The latter is

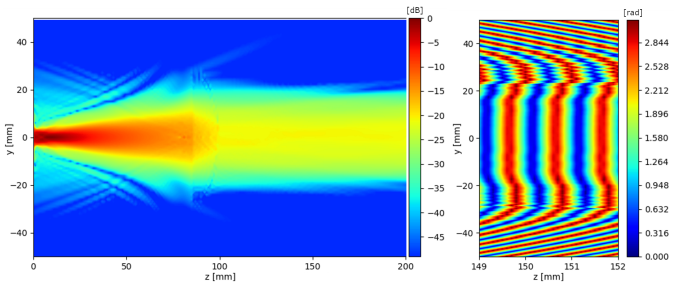

(a) Normalized intensity (dB) (b) Phase (rad)

Fig. 3. Normalized intensity and phase of the beam at the output of the GOLA.

operated by its digital twin through the RobotDK software and receives instructions from a Python script.

The robot employs positions specified in its base reference frame. Therefore, it is crucial to assess the orientation of the source's frame in relation to this base. Given the well-known shape of the diagonal horn antenna, multiple positions are measured on its surface using a calibration tool mounted on the robotic arm. These various positions generate a point cloud that can be analyzed to determine the z-axis of the source's frame and subsequently its optical axis. The same procedure is applied to the lens, as shown in Fig. 4.

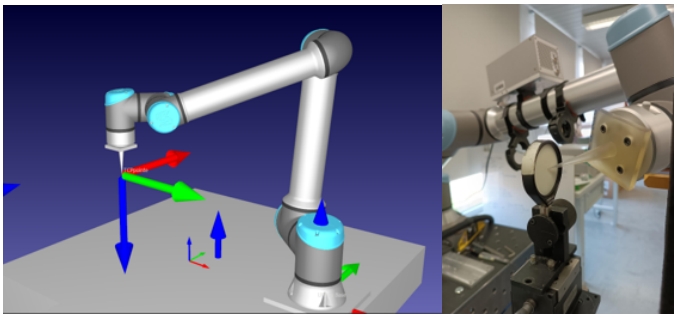

(a) Digital twin of the arm in cal-mode (b) Calibration tool

Fig. 4. Robot in the calibration mode.

After defining each frame, a second millimeter-wave converter, coupled with an open-ended rectangular waveguide (OEWG) probe, is mounted on the robotic arm (as depicted in Fig. 5). A Vector Network Analyzer (VNA) is used to capture and extract the four S-parameters from the millimeter-wave converters that feed both the horn and the probe.

This setup enables the measurement of both the intensity and phase of the electric field. Although it is a common practice to apply corrections to measurements obtained from an OEWG probe, please note that all measurements presented in this paper have not undergone correction yet.

The goal of this section is to demonstrate the validity of the results given by the simulation tool.

B. Measurements on the E-plane

The probe performs a scan of the yOz plane, initially along the z-axis and then towards the y-axis. The lens is positioned

Fig. 5. Collaborative robot measuring the field produced by a GOLA.

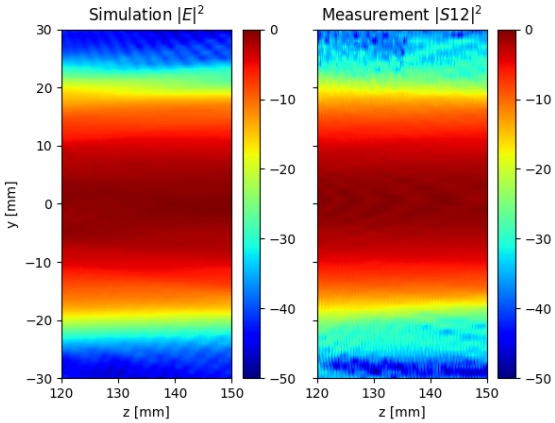

(a) Intensity ratio (dB).

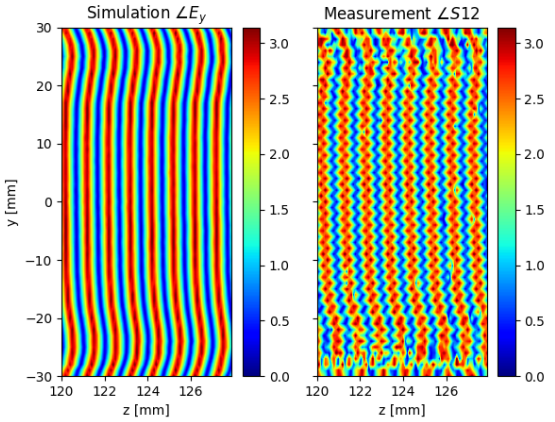

(b) Phase (rad).

Fig. 6. Comparison between the simulation and the measurements made on the E-plane.

at the optimal distance to generate a paraxial beam. Fig. 6 shows the results of a scan with a step size of 1λ for the y-axis and 0.1λ for the z-axis. There is a strong agreement between simulation and measurements in terms of intensity, and it is evident that the output beam is almost collimated. However, one can observe the presence of ripples in the phase that are not present in the simulation. Despite these ripples, the phase fronts follow a consistent pattern and remain nearly planar.

To investigate the source of these ripples, the same experiment was conducted without the lens, and the ripples persisted also in this case (see Fig. 7b). Additionally, Fig. 7c depicts the same scan but done in a reversed order, i.e. the y-axis is scanned before the z-axis. Interestingly, in this case, the ripples are absent. Hence, the way of moving the robot is crucial in preventing these positioning-related effects. The robot should move first along the axis with the larger step size, which is typically the transverse axis, as the phase varies rapidly at this frequency.

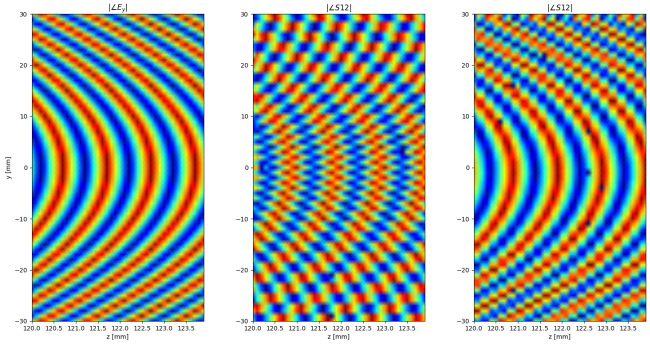

(a) Simulation (b) z-axis first (c) y-axis first

Fig. 7. Impact of the robot movements on the absolute phase.

C. Impact of a lens' offset and tilt

To verify whether the simulation tool can replicate the impact of a misalignment of the lens, a test is conducted where the probe is moved along the y-axis at a constant distance z from the source. The lens is positioned in front of the horn but is deliberately offset and tilted slightly. Its orientation is determined using the calibration tool. Subsequently, a simulation is carried out using this orientation as input, and its results are compared to the ideal scenario where no tilt occurs, as well as to the measurements obtained with the robotic arm.

As illustrated in Fig. 8, there is a strong agreement between the simulation and the measurement results.

IV. Conclusion

A suite of numerical tools, specifically tailored to handle the large electrical size of the system, has been employed to simulate the characterization bench. These simulation tools have been validated against measurements obtained with a robotic arm, demonstrating a strong level of agreement. Further comparisons are being conducted for more complex systems that involve mirrors and dielectric slabs.

In its calibration mode, the robotic arm enables a better alignment of lenses and other quasi-optical components by minimizing misalignment and offset. Nevertheless, it is important to carefully consider the robot's movement during

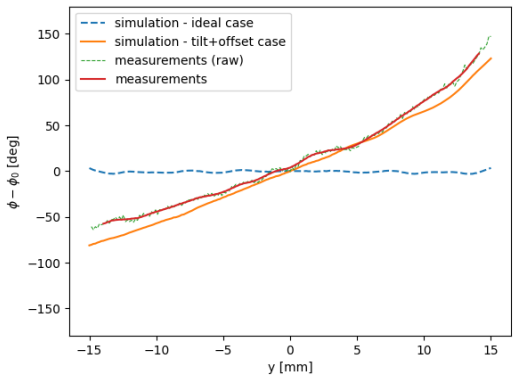

Fig. 8. Influence of lens displacement and angulation on the phase, comparison between the simulation result with measurement data.

measurements to prevent any disruptive effect. The robotic bench is currently used for conducting three-dimensional measurements by moving the probe and will be further employed in an imaging setup for moving the material under test instead of the probe.

References

[1] D. Bourreau et al., "A Quasi-Optical Free-Space Measurement Setup Without Time-Domain Gating for Material Characterization in the W-Band," IEEE Transactions on Instrumentation and Measurement, vol. 55, no. 6, pp. 2022–2028, Dec. 2006.

[2] P. F. Goldsmith, Quasioptical systems: Gaussian beam quasioptical propagation and applications. 1998.

[3] A. Chabory, J. Sokoloff, S. Bolioli, and P. F. Combes, "Computation of electromagnetic scattering by multilayer dielectric objects using Gaussian beam based techniques," Comptes Rendus Physique, vol. 6, no. 6, pp. 654–662, Jul. 2005.

[4] E. Kochkina, G. Wanner, D. Schmelzer, M. Tröbs, and G. Heinzel, "Modeling of the general astigmatic Gaussian beam and its propagation through 3D optical systems," Applied Optics, vol. 52, no. 24, p. 6030, Aug. 2013.

[5] J. A., J. R., and J. M., "Computer Aided Design of Waveguide Devices by Mode-Matching Methods," Passive Microwave Components and Antennas. InTech, Apr. 2010.

[6] D. Bourreau, G. Gaudin, A. Peden, "Modélisation et conception d'antennes à faisceaux gaussiens aux ondes millimétriques et submillimétriques, application à la caractérisation de matériaux et l'imagerie en bande J (220-330 GHz)," Journées Nationales Microondes (JNM), Limoges, France, Jun. 2022.

[7] J. Hillairet, "Applications du formalisme des faisceaux gaussiens à la modélisation de l'interaction d'une onde électromagnétique avec un objet 3D complexe," phdthesis, Université Paul Sabatier - Toulouse III, 2007.

[8] K. Elis, "Modélisation par faisceaux gaussiens de systèmes quasi-optiques intégrant des surfaces dichroïques pour la radiométrie millimétrique," phd, Université de Toulouse, Université Toulouse III - Paul Sabatier, 2012.

[9] A. Rohani, A. A. Shishegar, and S. Safavi-Naeini, "A fast Gaussian beam tracing method for reflection and refraction of general vectorial astigmatic Gaussian beams from general curved surfaces," Optics Communications, vol. 232, no. 1–6, pp. 1–10, Mar. 2004.